Platform Reagents Enable Synthesis of Ligand-Directed Covalent Probes: Study of Cannabinoid Receptor 2 in Live Cells

Miroslav Kosar,[a] David A. Sykes,[b] Alexander E. G. Viray,[c] Rosa Maria Vitale,[d] Roman C. Sarott,[a] Rudolf L. Ganzoni,[a] David Onion,[e] Janelle M. Tobias,[c] Philipp Leippe,[f] Christoph Ullmer,[g] Elisabeth A. Zirwes,[g] Wolfgang Guba,[g] Uwe Grether,*[g] James A. Frank,*[c,h] Dmitry B. Veprintsev,*[b] and Erick M. Carreira*[a]

[a]Laboratorium für Organische Chemie, Eidgenössische Technische Hochschule Zürich, Vladimir-Prelog-Weg 3, 8093 Zürich, Switzerland

[b]Faculty of Medicine & Health Sciences, University of Nottingham, Nottingham NG7 2UH, UK; Centre of Membrane Proteins and Receptors (COMPARE), University of Birmingham and University of Nottingham, Midlands, UK

[c]Department of Chemical Physiology & Biochemistry, Oregon Health & Science University, Portland, Oregon 97239-3098, United States

[d]Institute of Biomolecular Chemistry, National Research Council (ICB-CNR), Via Campi Flegrei 34, 80078 Pozzuoli, Italy

[e]School of Life Sciences, University of Nottingham, Nottingham NG7 2UH, UK

[f]Department of Chemical Biology, Max Planck Institute for Medical Research, Jahnstr. 29, 69120 Heidelberg, Germany

[g]Roche Pharma Research & Early Development, Roche Innovation Center Basel, F. Hoffmann-La Roche Ltd., 4070 Ba-sel, Switzerland

[h]Vollum Institute, Oregon Health & Science University, Portland, Oregon 97239-3098, United States

ABSTRACT

Pharmacological modulation of cannabinoid receptor type 2 (CB_2R) holds promise for the treatment of neuroinflammatory disorders, such as Alzheimer's disease. Despite the importance of CB_2R, its expression and downstream signaling are insufficiently understood in disease- and tissue-specific con-texts. Ligand-directed covalent (LDC) labeling enables the study of endogenously expressed proteins in living cells, tissues, and animals without impairment of native protein function. Herein, we employed in silico docking and molecular dynamics simulations to evaluate feasibility of LDC labeling of CB_2R and guide design of LDC probes. We demonstrate selective, covalent labeling of a peripheral lysine residue of CB_2R by exploiting fluorogenic O-nitrobenzoxadiazole (O-NBD) functionalized probes in a TR-FRET as-say. The rapid proof-of-concept verification with O-NBD probes inspired incorporation of advanced elec-trophiles suitable for experiments in live cells. To this end, novel synthetic strategies towards N-sulfonyl pyridone and N-acyl-N-alkyl sulfonamide LDC probes were developed, which allowed covalent delivery of fluorophores suitable for cellular experiments. The LDC probes were characterized in vitro by a radi-oligand binding assay and TR-FRET experiments. Application of the LDC probes in flow cytometry, imag-ing flow cytometry, and confocal fluorescence microscopy confirmed specific labeling of CB_2R in live cells.

INTRODUCTION

Cannabinoid receptors type 1 and 2 (CB_1R and CB_2R) are essential components of the endocannabinoid system (eCBS), which is of fundamental importance in a wide range of physiological processes in all vertebrates.[1,2] CB_1R is most abundant in the central nervous system, whereas CB_2R is expressed predominantly at the periphery by cells of the immune system.[3-5] Dysregulation of the eCBS, specifically of CB_2R signaling, has been implicated in numerous diseases including tissue injury, inflammation[6,7] and neurodegenerative conditions.[8,9] Despite early studies suggesting expression of CB_2R exclusively restricted to the periphery,[3,10,11] there is mounting evidence that CB_2R is expressed also in the brain.[12-16] Notably, brain glial cells, which play a crucial role in modulating immune response,[17] were found to express CB_2R.[18,19] Additionally, their significance was established in ameliorating neuroinflammatory diseases.[20,21]

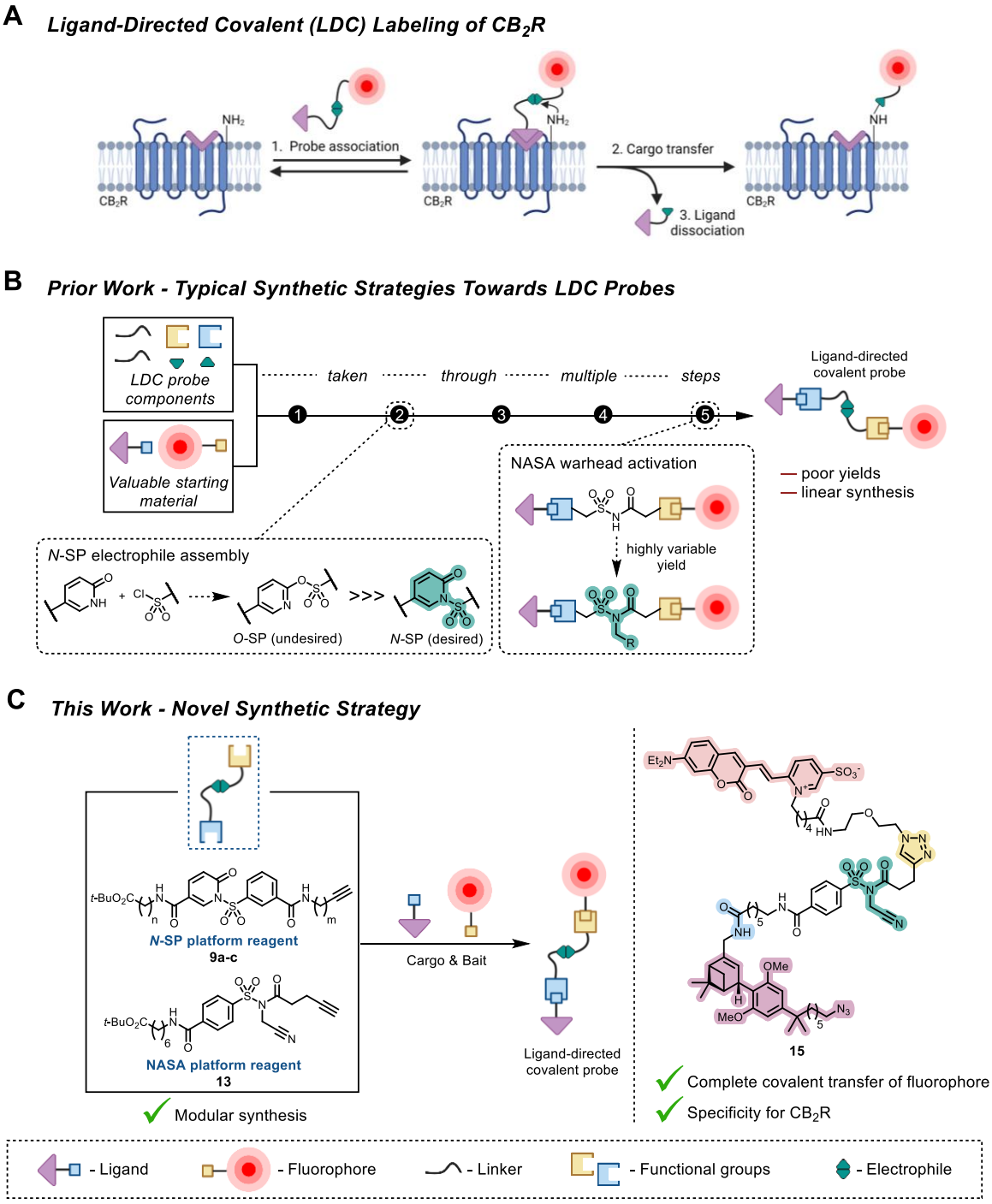

Figure 1. A Ligand-directed covalent (LDC) labeling of CB_2R. The process commences with affinity-driven association of the LDC probe with the receptor (1.), followed by proximity-driven covalent cargo transfer (2.) with concomitant dissociation of ligand from receptor (3.). **B** Comparison of typical prior strategies toward LDC probes using a linear functionalization of either ligand or fluorophore. **C** Herein reported work using a modular assembly with *N*-sulfonyl pyridone (*N*-SP) 9a-c and *N*-acyl-*N*-alkyl sulfonamide (NASA) 13 platform reagents.[22]

Expression of CB_2R is significantly upregulated under pathological conditions,[23,24] however, despite its evident importance, no therapeutics targeting the receptor selectively have been brought to the market. This shortcoming is largely attributed to poor understanding of receptor biology, in particular, its expression in tissue- and disease–dependent contexts. The situation is further complicated by the lack of specific antibodies,[25-28] scarcity of validated chemical probes,[29,30] and very low expression levels in native cells.[31-33]

Fluorescent probes have emerged as a powerful tool enabling the study of ligand-protein interactions with unrivaled spatiotemporal resolution.[34] Recently, our group has reported a potent CB_2R selective agonist scaffold, which was functionalized with a variety of fluorophores to enable visualization of CB_2R.[30,35] However, these probes are inherently limited in the study of native receptor biology, since they occupy the orthosteric ligand binding site. As such, they continuously exert their strong agonistic effects, which lead to disruption of cellular homeostasis and internalization of membrane-bound receptors.[33] Importantly, the fluorescent probe precludes binding by the respective endogenous ligands, perturbing the native state of CB_2R and associated downstream signaling. We surmised that these limitations could be addressed by introduction of cleavable, reactive motifs within the probe that transfer a fluorophore to the periphery of the protein of interest in a ligand-directed manner (Figure 1A). This strategy of affinity labeling, known as ligand-directed covalent (LDC) chemistry, allows for highly specific, fluorescent tagging of endogenously expressed proteins in complex, multimolecular systems.[36-38] The LDC process commences with nucleophilic attack by a proximal amino acid residue at the surface of the receptor. Following peripheral, covalent labeling, the ligand is free to dissociate from the binding site, and the native function of the receptor is preserved. This technique has been successfully applied to label both intracellular and membrane bound protein targets *in vitro*, in cells,[39-47] in brain slices,[48-50] and even in animals.[51]

In our continuing investigation of the eCBS, we recently became interested in developing LDC probes for CB_2R, for which no precedent is available. In this respect, we were inspired by the work of Hamachi, who has reported the use of *N*-sulfonyl pyridone[52] (*N*-SP) and *N*-acyl-*N*-alkyl sulfonamide[53] (NASA) motifs in LDC chemistry. Valuable ligands and fluorophores, which themselves may require challenging synthetic efforts, are frequently the starting materials for the

reported syntheses of LDC probes (Figure 1B). Additionally, during formation of the *N*-SP electrophile undesired *O*-SP constitutional isomer is formed preferentially leading to reduced yield. The starting materials are subjected to a long linear synthesis (up to 6-steps) and thus fall prey to the synthetic "arithmetic demon",[54] or diminution in material throughput incurred by a multi-step sequence.[55] Consequently, investigations of new protein targets often necessitate preparation of multiple probes and hence may be restricted to ligands or fluorophores available in sufficient quantities (grams), either from commercial sources or synthetic work.

We set out to devise new synthetic platforms for convergent and modular access towards LDC probes to enable broader applications and, specifically, for our studies of CB_2R in live cells (Figure 1C). The new approach has enabled the design and synthesis of *N*-SP and NASA platform reagents **9a-c** and **13**, which conveniently allow rapid assembly of LDC probes for CB_2R. Remarkably, the *N*-SP and NASA platform reagents we report can be coupled to free primary amines, despite the fact that these incorporate reactive electrophilic sites designed to trap *N*ε of lysine. We successfully demonstrate the suitability of our LDC probes to study CB_2R in live cells by flow cytometry, imaging flow cytometry, and fluorescence confocal microscopy. More broadly, the availability of the *N*-SP **9a-c** and NASA **13** platform reagents expands the targetable proteome and deliverable functionalities of LDC approaches by introduction of diverse bait and cargo elements late in the synthetic sequence.

RESULTS AND DISCUSSION

O-Nitrobenzoxadiazole: Rapid Proof-of-Concept by Fluorogenic Covalent Delivery

In general, an LDC probe consists of four components: high-affinity ligand, linker, reporter element and electrophilic motif, which can deliver the reporter and simultaneously release the ligand.[56,57] There are multiple challenges to the successful design of affinity labeling probes. A pitfall to be avoided is the introduction of a reporter element that adversely influences selectivity bias over closely related targets[58] or triggers significant decrease in affinity in comparison to the parent ligand.[59-61] Retention of high binding affinity is paramount as it may directly influence the rate of covalent cargo transfer.[53]

We have previously established the primary amine in **1a** as an optimal locus for linking ligand **1a** to a wide range of fluorophores (Scheme 1).[30,35] We opted to append agonist **1a** to an electrophilic motif subject to cleavage following ligand binding to the orthosteric site and reaction with a nearby lysine. Generally, selective modification of surface lysine residues is particularly challenging due to the high degree of solvation and low nucleophilicity.[62] Accordingly, we set out to investigate whether any lysine residues peripheral to the CB_2R binding site are amenable to covalent modification. In practice, we were attracted to *O*-linked nitrobenzoxadiazoles (NBD) **Ia-e** as they combine electrophile and reporter in a single motif. A key feature of **Ia-e** is that the alkyl *O*-linked NBDs are non-fluorescent, whereas *N*-linked NBDs formed upon reaction with alkyl amines (lysine residues) exhibit dramatic increase in fluorescence intensity.[63-65] This combination of electrophilic reactivity (via S_NAr) with fluorogenicity was seen as ideal to rapidly evaluate covalent modification. Furthermore, the small NBD unit combined with the distal nature of labeling site was expected to exert minimal impact on the endogenous activity of CB_2R.

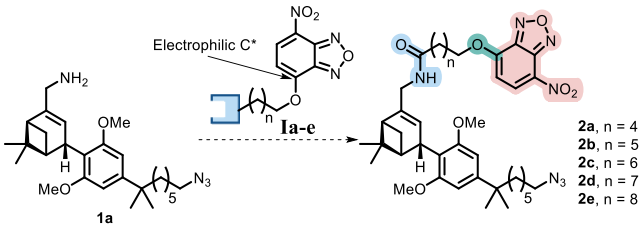

Scheme 1: Design of LDC *O*-NBD probes targeting CB_2R.

In Silico Probe Design & Molecular Dynamics Simulation

Examination of the co-crystal structure of CB_2R with agonist WIN55,212 (PDB:6PT0) revealed two lysines, namely $Lys23^{NTER}$ and $Lys103^{3.22}$ on the surface of CB_2R in proximity to the orthosteric binding site.[66] We used this structure in docking studies for the design of probes **2a-e** comprising **1a** and *O*-NBD. Prior work has highlighted the critical role of the linker type and length on the success as well as rate of target labeling.[45,63,67] This guided the selection of optimal linker length, which positions the electrophilic *O*-NBD carbon (C*) closest to the lysines. The hydrophobic lining of the exit channel from the orthosteric binding site suggested selection of alkyl

linkers. Consequently, CB_2R targeting appeared optimal with a heptanoyl linker (—$HNOC(CH_2)_6$—) featuring **2b**.

To gain further insight into the conformational preferences and binding mode of **2b**, we conducted two independent 1 μs molecular dynamics (MD) simulations using Amber20 program. Both inactive (MD1, PDB:5ZTY)[68] and active (MD2, PDB:6PT0)[66] conformations of CB_2R were used as starting points to enhance MD sampling and reduce potential biases from receptor conformation. The inactivating mutations present in PDB:5ZTY were back-mutated to wild-type residues before MD simulations. The same starting docking pose was used for both MD simulations since the conformation of the binding site is well-conserved in the two structures. The energy-minimized complexes were embedded in a pre-equilibrated palmitoyl-oleoyl-phosphatidyl-choline (POPC) lipid bilayer and solvated in an aqueous medium using the CHARMM-GUI web-interface.[69,70] Constant pressure and temperature (NPT) MD simulations were carried out at 310 K and 1 atm with the pmemd.cuda module of the Amber20 package,[71] using ff14SB (proteins), lipid 14 (lipids), and gaff (ligands) force field parametrizations (see SI for details).

Analysis of MD trajectories showed that **2b** adopts a canonical phytocannabinoid-like L-shaped conformation, forming van der Waals interactions with the hydrophobic residues lining the orthosteric site and engaging in π-π stacking with $Phe183^{ECL2}$. The amide group interacts with a network of water-mediated hydrogen bonds with $Asn93^{2.63}$, while the azide group, previously found critical to confer affinity and selectivity,[35] engages in polar interactions with $Thr114^{3.33}$ and $Tyr190^{5.39}$. The heptanoyl linker forms hydrophobic contacts with residues inside the helix bundle, while the *O*-NBD group docks on the extracellular rim of the helix bundle.

The rmsd analysis of MD1 and MD2 trajectories shows a similar trend in ligand fluctuations (see SI Figure S1). The fluctuations of **2b** and the ligand without linker (as the *N*-acetamide derivative of **1a**) were separately evaluated to uncouple the effect of the flexible linker from the rest of the molecule. Overall, the flexibility of the linker, mirrored by the increased fluctuation observed after its inclusion in the rmsd calculation, does not affect stability of the ligand within the orthosteric site. This suggests that the conjugate with NBD does not destabilize the ligand and that the linker provides adequate length to allow exiting the binding site without detrimental interactions between **2b** and CB_2R.

Subsequently, the propensity of the proximal lysine residues Lys23^{NTER} and Lys103$^{3.22}$ to adopt spatial arrangements suitable for nucleophilic attack was evaluated by monitoring the distance between electrophilic carbon C* in **2b** and the lysine *N*ε atoms (see SI Figure S2). In MD2 simulation the distance between the electrophile and either of the two lysines was similar. In contrast, however, two main conformational basins were identified in MD1 simulation where a transition was observed from an initial shorter distance between electrophile and Lys103$^{3.22}$ (Figure 2A) to Lys23^{NTER} (Figure 2B).

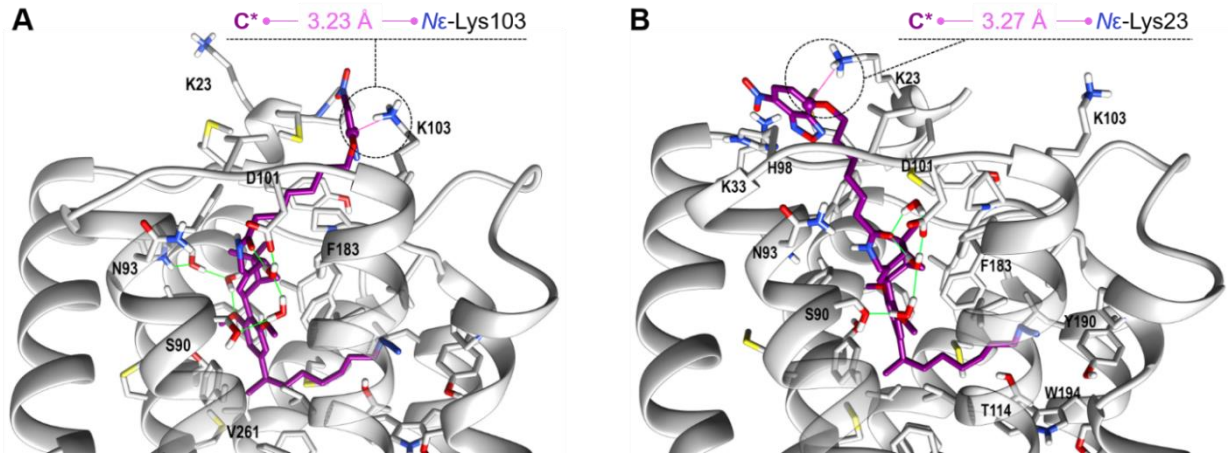

Figure 2. Representative frames from molecular dynamics simulation of 2b-CB2R complex (PDB:5ZTY) featuring the shortest distance between the electrophilic O-NBD carbon (C*) of 2b and Lys1033.22 (**A**) and Lys23NTER (**B**) Nε atoms.

The final conformation was stabilized by favorable interactions of the *O*-NBD group with CB_2R; π-π stacking of benzofurazan with His98^{ECL1} and a polar interaction between the nitro group and Lys33$^{1.32}$. This stabilized arrangement remained constant when the simulation was extended by further 300 ns. Notably, also in MD2 trajectory His98^{ECL1} remains close to the *O*-NBD group of **2b** for a large fraction of time (see SI Figure S3) while the stabilizing π-π stacking with benzofurazan is observed in two out of ten representative configurations arising from cluster analysis. In conclusion, although both Lys23^{NTER} and Lys103$^{3.22}$ in principle satisfy the requirements for them to act as nucleophiles, the data suggest that Lys23^{NTER} may react preferentially because for this pose the *O*-NBD group is locked in position by additional stabilizing interactions and polarized towards substitution.

Synthesis & Radioligand Binding Assay

We devised an efficient, convergent synthesis where **1a** was functionalized in the last step with the linker-reporter motif (Scheme 2). As such, a set of *O*-NBD probes **2a**-**e** was synthesized with linkers varying in carbon chain length from 6 to 10. For experiments that function as negative controls, *N*-NBD derivative **5** was synthesized. This probe is unable to transfer the NBD cargo and thus only labels CB_2R in a reversible fashion. Alkyl ω-hydroxy esters **3a**-**e** were allowed to react with F-NBD and the esters hydrolyzed under acidic conditions to reveal the carboxylic acid. Finally, HATU-mediated amide bond formation with **1a** at 0 °C afforded **2a**-**e**. Hence, *O*-NBD probes **2a**-**e** were obtained rapidly in three steps in a sufficient overall yield (28 – 38%). *N*-NBD control probe **5** was accessed in an analogous fashion starting from ester **4**.

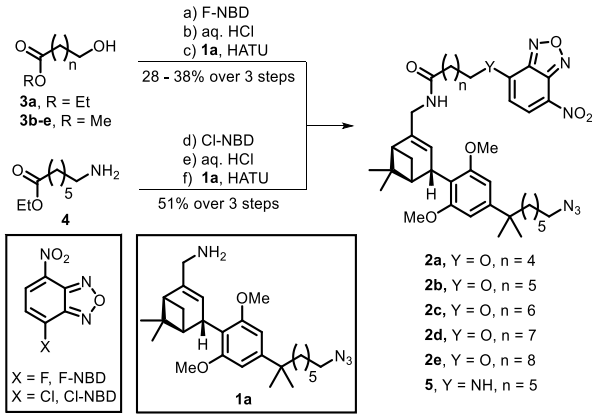

Scheme 2: Synthesis of *O*-NBD and *N*-NBD probes.[a]
[a]Reagents and conditions: (a) F-NBD, Et_3N, DMAP, CH_2Cl_2, rt, 40 – 61%; (b) aq. HCl, dioxane, 100 °C, 81 – 93%; (c) 1a, HATU, *i*-Pr_2NEt, DMF, 0 °C – rt, 76 – 90%; (d) Cl-NBD, $NaHCO_3$, MeOH, rt, 92%; (e) aq. HCl, dioxane, 100 °C, 83%; (f) 1a, HATU, *i*-Pr_2NEt, DMF, rt, 67%.

The *in vitro* pharmacological profile of *O*-NBD probes **2a**-**e** was evaluated in radioligand competition binding studies using [^{3}H]CP55,940 and membrane preparations of Chinese hamster ovary (CHO) cells expressing human CB_1R (hCB_1R), CB_2R (hCB_2R) or mouse CB_2R (mCB_2R) (Table 1.). All probes **2a**-**e** emerged as high affinity binders for hCB_2R with K_i values of 53 nM, 49 nM, 91 nM, 55 nM and 74 nM, respectively. Probes **2a**-**e** were avid binders of mCB_2R, albeit with decreased potency in comparison to the hCB_2R ortholog. Probes **2b**, **2d** and **2e** also demonstrated excellent selectivity over the closely related hCB_1R (hK_i ratio $CB_1R/CB_2R > 100$).

These data validate the *in silico*-guided probe design, which yielded probes with excellent *in vitro* binding profiles.

Table 1. Radioligand competition binding assay of *O*-NBD LDC probes.[†]

Cpd.	n	K_i [nM]			
		hCB_1R	hCB_2R	mCB_2R	hK_i ratio (CB_1R/CB_2R)
2a	4	5207	53	198	98
2b	5	6039	49	443	123
2c	6	4130	91	377	45
2d	7	>10000	55	641	>182
2e	8	>10000	74	351	>135

[†][^{3}H]-CP55,940 was used to establish affinity (K_i) values in the radioligand binding assay with membrane preparations from CHO cells overexpressing hCB_1R, hCB_2R, or mCB_2R.

The pattern of molecular interactions observed during MD simulations provides insight for the observed trend involving stronger binding of **2a-e** toward hCB_2R over the mouse ortholog. This could be ascribed to the human to mouse Val261$^{6.51}$Ala, Ser90$^{2.60}$Asn and Asn93$^{2.60}$Ile amino acid replacements. Val261$^{6.51}$ sidechain forms stabilizing hydrophobic interactions with the dimethyl group of the azidoheptyl substituent on the arene, which are absent in the mouse ortholog incorporating an alanine residue. Ser90$^{2.60}$Asn and Asn93$^{2.60}$Ile substitutions alter the steric hindrance of the ligand binding site and disrupt the network of water-mediated H-bonds, respectively. The drastic drop in affinity observed toward CB_1R cannot be fully explained by the CB_2R and CB_1R amino acid residue substitutions alone. Thus, we speculate that significant contributions arise from the differences in ligand accessibility to the CB_2R versus CB_1R binding sites, as reported for the parent ligand of **1a**, HU-308.[72]

TR-FRET Based Assay to Assess Covalent NBD Transfer to CB_2R

The binding data for **2a-e** suggest that conjugation of **1a** with the electrophilic *O*-NBD motif is well tolerated. In previous work on ligand directed chemistry, covalent labeling was validated by Western blotting,[53] mass spectrometry,[44,73,74] UV-Vis spectroscopy[63] or time-resolved Förster resonance energy transfer (TR-FRET).[75] All of these approaches suffer from disadvantages. Western blotting along with mass spectrometry can be laborious and omit early time points, with

the latter suggesting erroneous labeling rate for rapid reactions and resulting in inaccurate information of required incubation time. The use of UV-Vis spectroscopy can inform on the type of modified residue, however, its use is limited to reactions wherein covalent transfer leads to changes in spectral properties. The TR-FRET experiments as applied previously[75] do not give real-time insight into the rate of covalent labeling nor suggest the amino acid residue being modified.

To improve on the shortcomings of the reported methods, we aimed to exploit the spectral differences between *O*-NBD and *N*-NBD in combination with the temporal resolution offered by TR-FRET (Figure 3A). As such, covalent labeling could be monitored in real time from the very start of the experiment following probe addition. As an added benefit, the intensity and wavelength of emission would inform on the type of residue involved in the covalent modification. In our TR-FRET binding assay, membrane preparations of human embryonic kidney cells (HEK293) overexpressing SNAP-tagged CB_2R were labeled with a terbium-based FRET donor (SNAP-Lumi4-Tb). Upon irradiation ($\lambda = 337$ nm), the Tb donor initiates energy transfer to a proximal fluorescence acceptor and the measured acceptor to donor emission ratio provides direct insight into the covalent labeling. Since probes **2a**-**e** carry an alkyl *O*-NBD group and are hence non-fluorescent,[64,65] increase of emission at $\lambda_{em} = 520$ nm indicates covalent *O*- to *N*- transfer of NBD.

Incubation of SNAP-CB_2R membrane preparation with **2b** led to gradual increase of the FRET emission ratio (Figure 3B). Addition of a validated CB_2R antagonist/inverse agonist, SR-144,528 (hCB_2R K_i = 13 nM),[76] following 120 min incubation did not lead to decrease in the signal intensity, corroborating successful NBD covalent transfer to a lysine residue.

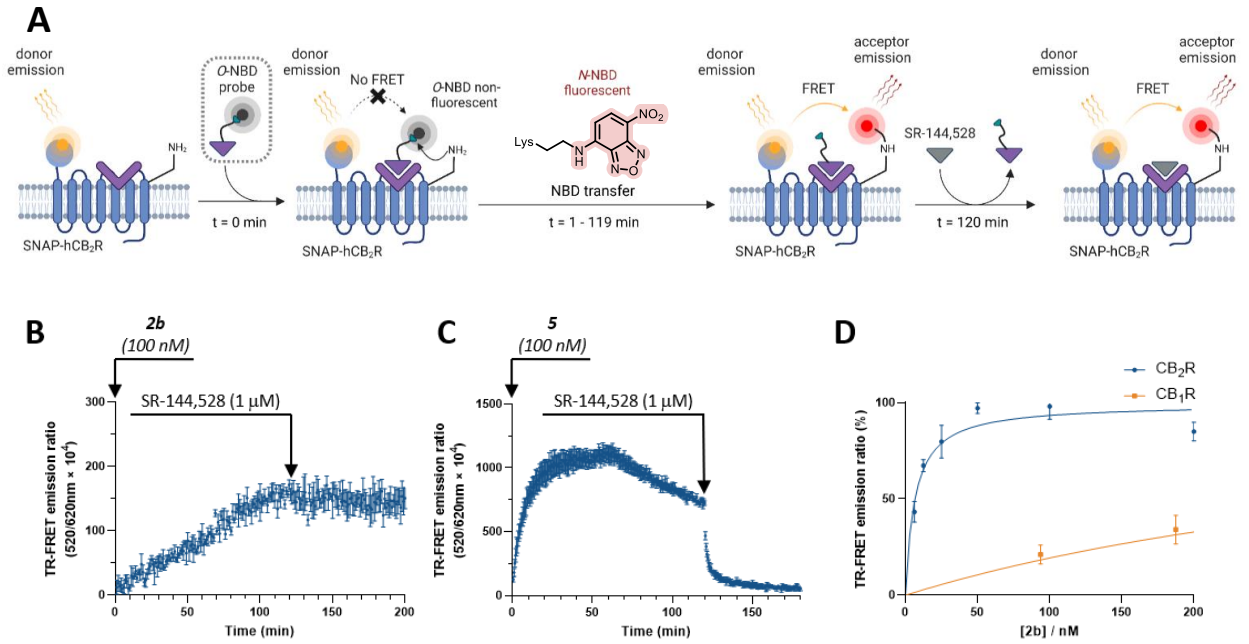

Figure 3. TR-FRET based characterisation of covalent NBD transfer to CB_2R; **A** Schematic flowchart of the TR-FRET experiment to investigate cargo transfer of *O*-NBD probes 2a-e.[22] **B** SNAP-Lumi4-Tb labelled CB_2R membranes were treated with *O*-NBD probe 2b (100 nM). Following incubation for 120 min at 25 °C SR-144,528 (1 µM) was added. **C** SNAP Lumi-4-Tb labelled CB_2R membranes were treated with *N*-NBD probe 5 (100 nM). Following incubation for 120 min at 25 °C SR-144,528 (1 µM) was added. **D** Saturation binding profile following a 2 h incubation at 37 °C with 2b using a membrane preparation of HEK293 cells expressing either CB_1R or CB_2R, previously labelled with SNAP-Lumi4-Tb.

Probe **2a** achieved reduced signal intensity in comparison to **2b**, likely owing to its short linker (see SI Figure S4). As seen for **2b,** probes **2c-e** also demonstrated good covalent labeling efficiency (see SI Figure S4). From this set, **2b** was deemed optimal for our investigations due to its excellent affinity and selectivity for CB_2R in the radioligand study combined with the strong signal in the TR-FRET assay. Additionally, the shorter, less lipophilic linker of **2b** was expected to result in improved target specificity in comparison to **2c-e**.

As a control experiment, an analogous study was performed with probe **5**, which features identical ligand and heptanoyl spacer as **2b**. However, it is incapable of undergoing transfer because it features an *N*-linked NBD fluorophore (Figure 3C). Incubation with **5** led to an increase in the FRET emission ratio (receptor binding), however, the addition of SR-144,528 dramatically decreased the signal intensity. This observation implies that probe **5** was displaced in a competitive

fashion following SR-144,528 addition. These results collectively suggest that the ligand for the CB_2R binding site can be displaced from the orthosteric binding site following NBD transfer by **2b**. The novel fluorogenic aspect applied in the TR-FRET assay enables rapid validation that a lysine residue proximal to the binding site of CB_2R is amenable to covalent modification.

Upon further profiling, *O*-NBD probes were not susceptible to hydrolysis (pH = 1 – 8, see SI Table S1). We also set out to investigate whether the excellent selectivity of **2b** established by radioligand binding as shown in Table 1, would be reflected in the TR-FRET assay. Measurement of saturation binding following 2 h incubation at 37 °C with the respective CB_1R or CB_2R membrane preparations revealed a 50-fold selectivity bias of **2b** for CB_2R over CB_1R, which is in agreement with the radioligand binding assay (Figure 3D).

Universal Cargo Delivery Platform - *N*-Sulfonyl Pyridone & *N*-Acyl-*N*-Alkyl Sulfonamide

Synthetic Design

The *O*-NBD probe **2b** demonstrated that covalent cargo transfer to a lysine residue of CB_2R is feasible. However, owing to the intrinsic reactivity of **2b**, modification is exclusively restricted to covalent introduction of an NBD fluorophore. In this respect, the photophysical properties of the NBD fluorophore are suboptimal for cellular experiments due to its low quantum yield and tendency to photobleach.[77] Accordingly, we aimed to expand the repertoire of deliverable cargos, introduce a handle to tailor physicochemical properties, and design probes suitable for experiments in live cells.

In 2017 the Hamachi group reported ligand-directed sulfonylation of tyrosine and lysine residues facilitated by *N*-sulfonyl pyridones (*N*-SP).[52] Despite the attractiveness of the system, to the best of our knowledge, this is the only report utilizing LDC *N*-SP probes. We suspect that a significant hurdle to broader adoption of the *N*-SP chemistry is the currently available synthetic route. It suffers from a number of limitations, including linearity, production of undesired *O*-pyridone constitutional isomers, and poor yields overall.

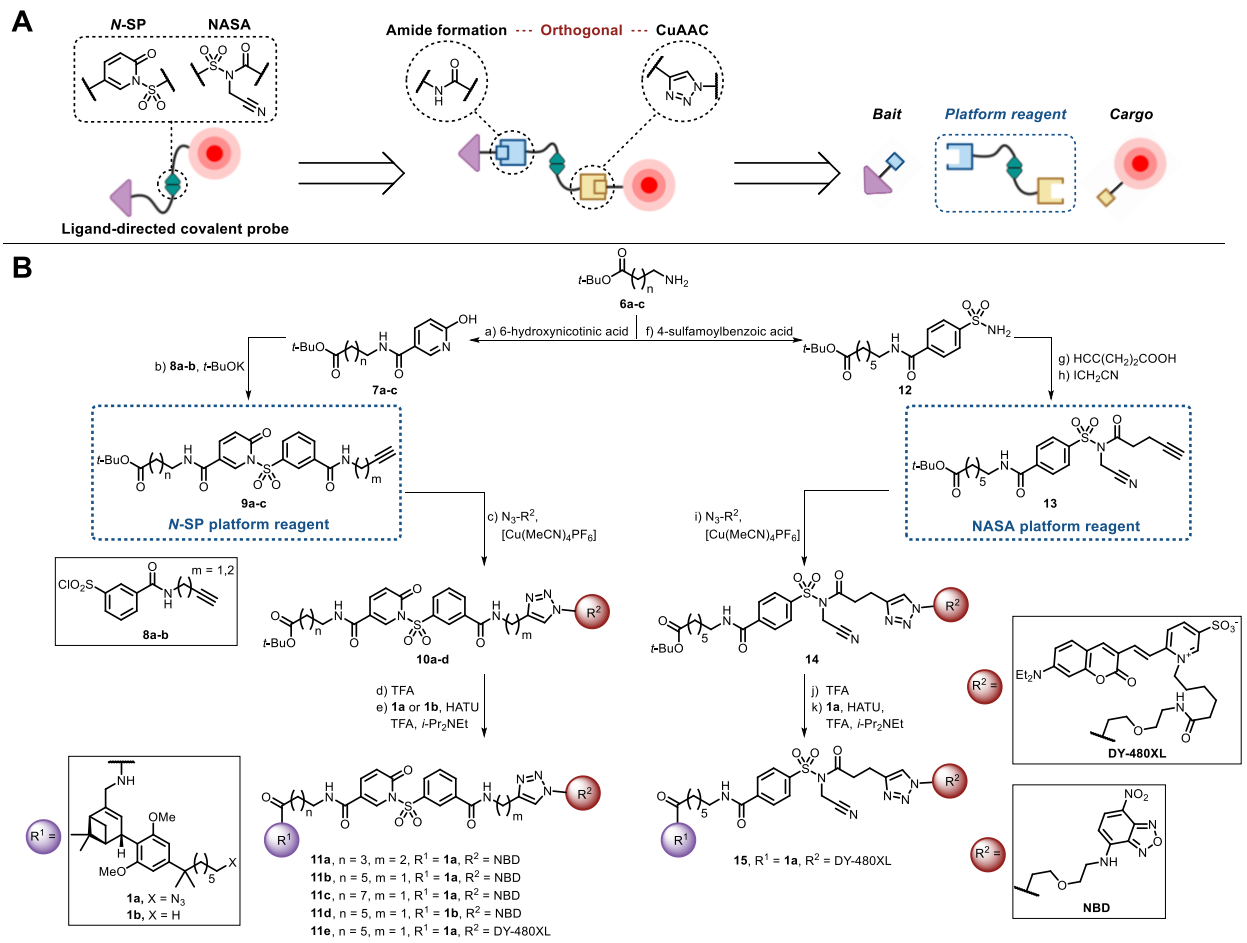

Scheme 3. A Proposed disconnection of *N*-SP and NASA LDC probes to their respective platform reagents. **B** Synthesis of *N*-SP and NASA probes.[a]

[a]Reagents and conditions: (a) 6-hydroxynicotinic acid, EDCI·HCl, Et_3N, DMF, rt, 67 – 87%; (b) 8a or 8b, *t*-BuOK, THF, −78 °C to rt, 68 – 72%; (c) N_3-DY-480XL or N_3-NBD, $[Cu(MeCN)_4]PF_6$, AcOH, CH_2Cl_2, rt, 73 – 88%; (d) TFA, CH_2Cl_2, rt; (e) 1a or 1b, HATU, TFA, *i*-Pr_2NEt, DMF, 0 °C to rt, 72 – 92% over two steps; (f) 4-sulfamoylbenzoic acid, EDCI·HCl, HOBt·H_2O, *i*-Pr_2NEt, DMF, rt, 67%; (g) 4-pentynoic acid, EDCI·HCl, DMAP, *i*-Pr_2NEt, DMF, rt, 70%; (h) ICH_2CN, *i*-Pr_2NEt, DMF, rt, 78%; (i) N_3-DY-480XL, $[Cu(MeCN)_4]PF_6$, AcOH, CH_2Cl_2, rt, 94%; (j) TFA, CH_2Cl_2, rt; (k) 1a , HATU, TFA, *i*-Pr_2NEt, DMF, 0 °C to rt, 66% over two steps.

N-Acyl-*N*-alkyl sulfonamide (NASA) constitutes a complementary electrophile for covalent linking. It is selective for ligand-directed acylation of lysine residues and has lately been the electrophile of choice due to its rapid labeling kinetics (k_2 = 10^4 M^{-1} s^{-1}).[53] The application of NASA electrophiles includes generation of small-molecule LDC probes,[53,78] LDC aptamers,[79] development of ligand screening assays,[80] modification of protein-protein interactions[81] and

targeted protein degradation.[82] In many of the reported cases, the synthesis of the LDC probes commenced from precious starting materials which are subjected to laborious synthesis sequences. Consequently, the resulting applications may be restricted to conveniently available ligands and fluorophores.

In a single instance,[52] Hamachi reported amide bond formation in presence of the *N*-SP electrophile followed by a copper-catalyzed azide-alkyne cycloaddition (CuAAC) to assemble the LDC probe albeit in 2% yield over the two steps.[52] We thus hypothesized that further investigations could yield methods to assemble LDC probes incorporating either *N*-SP or NASA electrophiles by robust orthogonal functionalization in the final steps with cargo and ligand. Hence, we envisioned a streamlined assembly route for probes involving central *N*-SP and NASA platform reagents (Scheme 3A). This strategy significantly expands the available targets that can be engaged as well as the range of deliverable cargos by allowing a wide range of ligands and fluorophores to be efficiently incorporated into the LDC probes. The availability of fluorophores bearing azides and ligands incorporating amines suggested the use of CuAAC and amide bond formation, respectively.

Synthesis of the LDC probes commenced with ω-amino alkyl esters **6a-c** (Scheme 3B). *En route* towards *N*-SP platforms, the esters were allowed to react with 6-hydroxynicotinic acid to yield 6-hydroxynicotinamides **7a-c**. The reported conditions for the formation of *N*-SP using triethylamine in DMF[52] yielded a 3:1 mixture favoring the undesired *O*-SP over the *N*-SP constitutional isomer, consistent with the low yields reported by Hamachi.[52] Further investigations by us led to conditions in which the *N*-SP constitutional isomer is formed preferentially using *t*-BuOK in THF at –78 °C (*O*-SP : *N*-SP = 1:10) in good yield (68 – 72%) to give platform reagents **9a-c**.

Complementary NASA platform reagent **13** was accessed rapidly in three steps by reacting **6b** with 4-sulfamoylbenzoic acid to yield **12**, followed by *N*-acylation with 4-pentynoic acid and finally *N*-alkylation with iodoacetonitrile. Platform reagents **9a-c** and **13** were functionalized with fluorophores by CuAAC to yield **10a-d** and **14**, respectively. During the final amide bond formation with the targeting ligand *N*-SP and NASA electrophilic motifs are highly susceptible to degradation, therefore efficient activation of the carboxylic acid, produced following ester deprotection in **10a-d** and **14**, was required for a rapid and selective reactivity with amines.

Unfortunately, many methods for the activation of carboxylic acids are either too harsh or involve nucleophiles (e.g. DMAP, HOBt) that can facilitate degradation of the *N*-SP and NASA motifs. We noted that the amide bond can be formed selectively in presence of the highly electrophilic *N*-SP and NASA motifs by employing HATU in a TFA/*i*-Pr_2NEt mixture that serves to buffer out the nucleophilic HOAt. This discovery allowed us to complete the modular synthesis and link the CB_2R homing ligands **1a-b** to yield the respective *N*-SP (**11a-e**) and NASA (**15**) probes.

TR-FRET Based Assay to Evaluate Covalent Transfer of *N*-SP & NASA LDC Probes

We have subsequently tested efficiency of probes **11a-e** and **15** towards transfer of their cargo by means of TR-FRET. Each probe was tested with analogous experiments previously described for **2b** (Figure 3A): incubation of CB_2R membrane preparation with probe, followed by addition of SR-144,528 to dissociate unreacted probe (see Figure 4 and SI Figures S5-S7). We evaluated the efficiency of covalent modification as the ratio of FRET intensity prior to addition of SR-144,528 to the FRET intensity post addition at the end of measurement.

Variation in the spacer length separating the ligand and *N*-SP electrophile yielded probes with pentanoyl (**11a**), heptanoyl (**11b**) and nonanoyl (**11c**) exit vectors. Upon incubation with the membrane preparation for 120 min at 25 °C, the probes demonstrated efficiency of covalent labeling of 11.3% ± 2.7%, 13.6% ± 1.9% and 9.8% ± 3.4%, respectively. Probe **11d** was prepared from ligand **1b** where the terminal azide, which was previously shown to increase affinity for CB_2R by up to 15-fold,[35] was deleted. Accordingly, **11d** demonstrated reduced covalent transfer (3.8% ± 6.4%) within the 120 min incubation time and corroborated the affinity-driven nature of our labeling approach. *N*-SP probe **11e** bearing a red-shifted DY-480XL dye with large Stokes shift (see SI Figure S8) suitable for *in vivo* imaging demonstrated decent covalent transfer in 120 min (25.2% ± 1.4%).

When the incubation time of probes **11a-e** was extended to 20 h the labeling yields significantly improved (**11a** = 46.9% ± 3.2%, **11b** = 49.6% ± 1.8%, **11c** = 59.6% ± 3.8%, **11d** = 37.5% ± 2.7%). Notably, following 20 h incubation time, **11e** demonstrated complete covalent transfer of its fluorophore, as indicated by our FRET assay (105.7% ± 7.2%). When the experiment was performed at a physiologically relevant temperature (37 °C) the rate was enhanced and **11e** showed 53.5% ± 9.6% cargo transfer after 120 min. By measuring saturation binding we were pleased to

see that **11e** demonstrated a 119-fold selectivity for CB_2R over CB_1R in our TR-FRET assay (see SI Figure S9).

Finally, switching the *N*-SP electrophile of **11e** to the more reactive NASA motif yielded probe **15**. Accordingly, the modification greatly improved the rate of covalent labeling and **15** achieved complete transfer (100.8% ± 4.1%) within the 120 min incubation time at 37 °C.

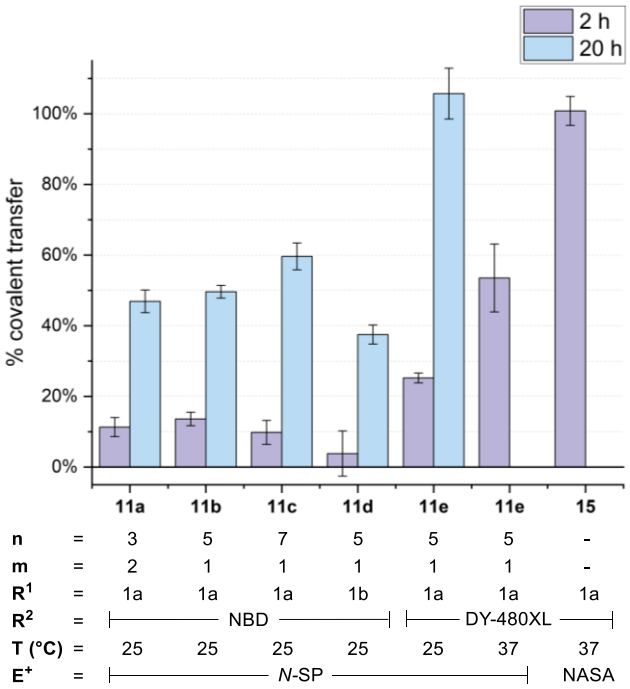

Figure 4. TR-FRET based evaluation of covalent cargo transfer of probes 11a-e (100 nM, 25 °C) and 15 (200 nM, 37 °C) following a 2 h or 20 h incubation. The percentage shown for each probe represents a quotient of its TR-FRET ratio determined prior to addition of SR-144,528 and at the end of measurement post addition. Mean ± SEM, $N = 3$

Molecular Dynamics Simulation of Probe 15

Subsequently, the best performing probe **15** was investigated by MD simulations. The conformational space accessible to the NASA linker of **15** and its molecular interactions within the ligand binding site were explored with two independent 1 μs MD simulations to identify residues that could serve as nucleophiles. The simulations were run with the same computational protocol adopted for **2b**, using a truncated form of **15** in which the fluorophore was deleted, implied stable binding of the probe in the orthosteric site (see SI Figure S10). The MD1 and MD2 simulations were in agreement in finding that both $Lys23^{NTER}$ and $Lys103^{3.22}$ are at suitable

distances for acylation (see SI Figures S11–S13). Furthermore, due to greater linker length and flexibility, the NASA electrophile is also in proximity to Lys33$^{1.32}$ (see SI Figures S14–S15). In the simulations, His98^{ECL1} stabilized the linker by forming either direct or water-mediated hydrogen bonds with the NASA group. Moreover, His98^{ECL1} remained spatially close to the NASA electrophile over a considerable fraction of the simulated period suggesting it could assist in the covalent modification of CB_2R by **15** (see SI Figure S15).

Conventional and Imaging Flow Cytometry with LDC Probes in CB_2R Expressing Live Cells

Having established the success of covalent cargo transfer of the probes and target specificity *in vitro*, we next turned our attention to investigate labeling of CB_2R in live cells. The best performing probes of each electrophile type, namely *O*-NBD (**2b**), *N*-SP (**11e**) and NASA (**15**), were studied by means of conventional and imaging flow cytometry. Conventional flow cytometry (FC) allows rapid quantitative assessment of total cells fluorescence and imaging flow cytometry (IFC)[83] additionally yields quantitative information about localization of a fluorophore across 10,000 cells.

To this end, HEK293 T-REx cells expressing hCB_2R along with HEK293 wild-type cells (no CB_2R expressed) were incubated with an LDC probe at concentrations that ranged from 6.25 nM – 200 nM and subsequently analyzed by means of FC. The FC data of probes **2b**, **11e** and **15** implied significantly increased fluorescence intensity in cells expressing hCB_2R (Figure 5A, SI Figures S16A and S17A) in comparison to wild-type cells (Figure 5B, SI Figures S16B and S17B). Furthermore, the fluorescence signal of all three probes was substantially reduced upon pre-incubation with SR-144,528 implying excellent CB_2R binding specificity in a cellular setting. *O*-NBD probe **2b** demonstrated clear specific binding signal in CB_2R expressing cells when compared to wild-type. However, the signal was relatively weak and fairly high levels of non-specific binding were detected upon pre-incubation with SR-144,528. *N*-SP and NASA probes **11e** and **15** displayed excellent specific binding in CB_2R expressing cells with minimal background signal in cells pre-incubated with SR-144,528. For both **11e** and **15** the fluorescent signal was substantially more intense in comparison to **2b** and their target engagement was highly specific in CB_2R expressing cells with virtually no binding in the wild-type cells.

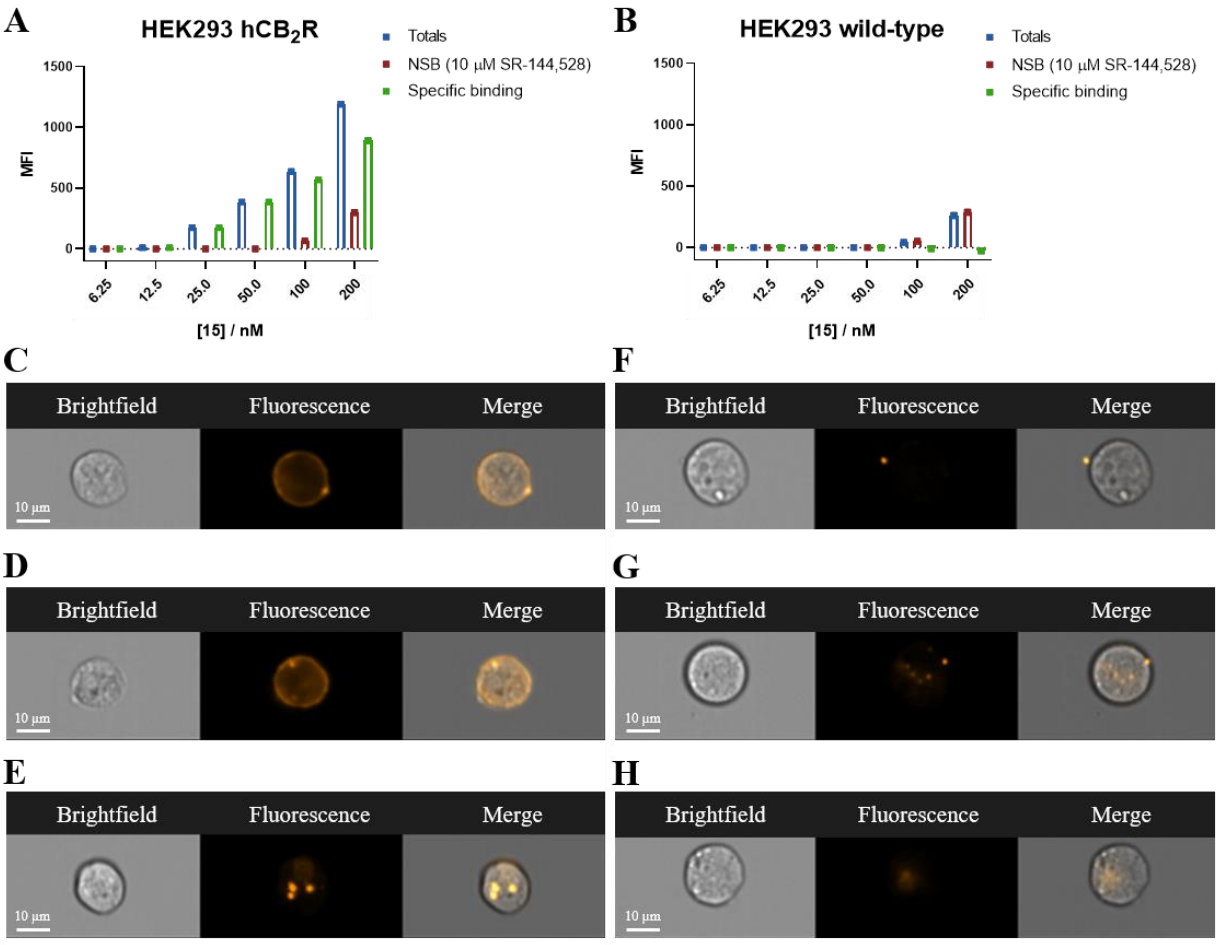

Figure 5. Conventional and imaging flow cytometry studies with LDC probe 15; Conventional flow cytometry of HEK293 T-REx hCB$_2$R (**A**) and HEK293 wild-type cells (**B**) upon incubation with 15 (6.25 – 200 nM). The mean fluorescence intensity (MFI) is shown with subtracted background. Representative frames from imaging flow cytometry experiments using HEK293 T-Rex hCB$_2$R and 15 (210 nM) with CB$_2$R visualized primarily at the plasma membrane (**C**, MIQ < –1), at both membrane and intracellularly (**D**, MIQ = –0.5 – 0.5), and intracellularly (**E**, MIQ > 2). The same experiment with cells pre-incubated with SR-144,528 (10 µM) showing fluorescence restricted to the plasma membrane (**F**, MIQ < –1), at both membrane and intracellularly (**G**, MIQ = –0.5 – 0.5), and intracellularly (**H**, MIQ > 2). Median internalization quotient (MIQ) compares internal to whole cell fluorescence, where smaller number corresponds to less CB$_2$R internalization. For additional exemplary frames, histograms and analysis see SI.

Complementary IFC experiments allowed us to validate binding specificity and distinguish CB$_2$R visualized intracellularly in comparison to receptors restricted to the plasma membrane. Live HEK293 T-REx cells expressing hCB$_2$R were incubated with either **2b**, **11e** or **15** (see SI

Figures S18–S21). The results were compared to cells pre-incubated with SR-144,528 before addition of the LDC probe. The average of the 10,000 generated cellular images was interrogated to yield an overall representation of binding specificity and localization of labeling.

In agreement with results from the conventional FC experiments, all three probes **2b**, **11e** and **15** demonstrated labeling in hCB$_2$R expressing cells (Figure 5CDE, SI Figures S18AB, S19ABC and S20ABC) which was substantially reduced in cells pre-incubated with SR-144,528 (Figure 5FGH, SI Figures S18CD, S19DEF and S20DEF). The fluorescence intensity for **2b** was 1.9-fold greater in comparison to control and was reduced by 16% in cells pre-incubated with SR-144,528 as determined by median fluorescence intensity (MFI) (see SI Figure S22 and Table S2). Compared to control, DY-480XL functionalized probes **11e** and **15** showed 9.4-fold and 8.5-fold increase in fluorescence intensity, respectively (see SI Figures S23-S24 and Table S3). The fluorescence signal of **11e** and **15** was reduced in cells pre-incubated with SR-144,528 by 38% and 52%, respectively, as determined by MFI.

Subsequently, we analyzed individual images of the whole gated cell population to discern populations of internalized and membrane bound CB$_2$R. Median internalization quotient (MIQ) was used to compare internal to whole cell fluorescence, where a smaller number indicates less CB$_2$R internalization (see SI for details). Incubation with **2b** visualized CB$_2$R localized at the membrane and intracellularly to a similar extent with MIQ = 0.91. Compared to **2b**, cells exposed to **11e** or **15** demonstrated receptor internalization to a smaller degree and visualized CB$_2$R primarily confined to the plasma membrane with MIQ = 0.46 and MIQ = 0.68, respectively.

Collectively, the data showcase the high affinity and excellent specificity of LDC probes **2b**, **11e** and **15** for CB$_2$R in living cells. Moreover, the DY-480XL functionalized **11e** and **15** displayed intense fluorescent signal and allowed bright visualization of CB$_2$R, attesting to their suitability for application in cellular settings.

Fluorescence Confocal Microscopy with LDC Probe 15 in Live Cells

Due to the relatively high lipophilicity of CB$_2$R ligands, we wanted to verify in an independent experiment that our probes were labeling CB$_2$R, as opposed to accumulating non-specifically within the cellular membranes. We therefore used lentiviral transduction to produce a cell line stably expressing hCB$_2$R *N*-terminally fused to a SNAP-tag [AtT-20(SNAP-hCB$_2$R)]. Live AtT-20(SNAP-hCB$_2$R) cells were co-incubated with **15** (2 μM), SNAP-Surface-649 (100 nM) to

fluorescently label the SNAP-tags, and Hoechst-33342 (100 nM) to label the nuclei, for 45 min; then the cells were imaged by confocal fluorescence microscopy (see Figure 6 and SI Figure S25).

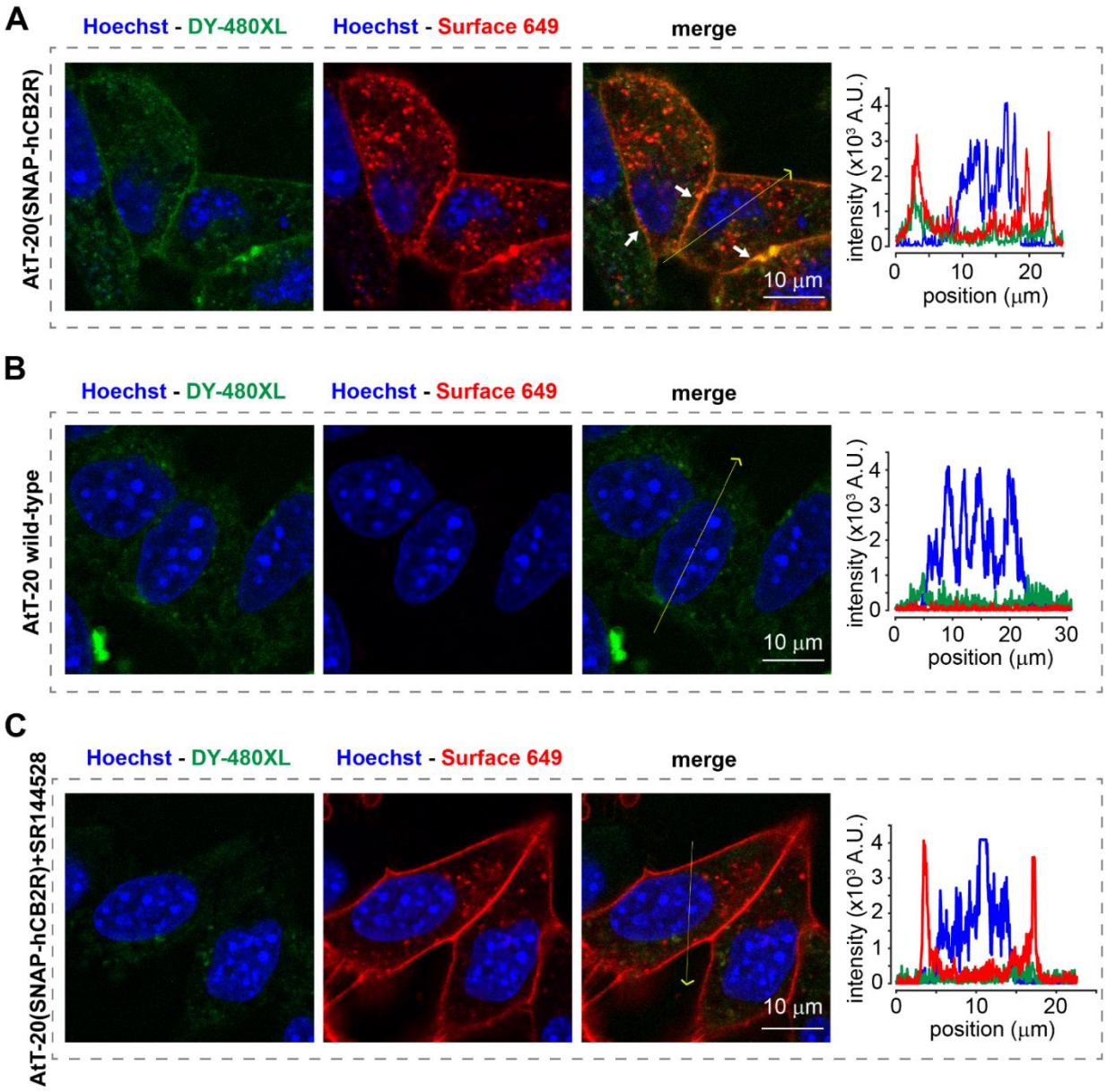

Figure 6. Fluorescence confocal microscopy with LDC probe 15; Fluorescent labeling of CB_2R using 15 (2 µM) to deliver DY-480XL by LDC in (**A**) AtT-20(SNAP-hCB_2R) cells, (**B**) AtT-20-wild-type cells, and (**C**) AtT-20(SNAP-hCB_2R) cells that were pre-treated with the CB_2R antagonist SR-144,528 (20 µM). Nuclei were stained with Hoechst33342 and white arrows highlight CB_2R and SNAP-dye plasma membrane colocalization. Right panels indicate the intensity profile across the yellow line for Hoechst33342, DY-480XL fluorescence, and SNAP-Surface-649.

We observed a strong DY-480XL signal on the plasma membrane of the cells, as well as puncta intracellularly, which could represent internalized receptors (Figure 6A, left). This signal co-localized with the far-red SNAP-dye signal (Figure 6A, right), confirming that **15** was successfully labeling the SNAP-tagged CB_2Rs.

Applying the same treatment to wild-type AtT-20 cells, which do not express CB_2Rs or SNAP-tags, resulted in a lack of DY-480XL or SNAP-Surface-649 at the plasma membrane, confirming that the dyes are labeling surface-expressed SNAP-hCB_2R (Figure 6B). To verify that **15** was labeling CB_2R by binding its orthosteric site, AtT-20(SNAP-hCB_2R) cells were pre-treated with SR-144,528 (20 μM), followed by **15**, SNAP-Surface-649, and Hoechst-33342 as before. Pre-treatment with SR-144,528 abolished the DY-480XL signal on the plasma membrane, while the SNAP-tags were still observed on the plasma membrane (Figure 6C). Combined, these results confirm that in living cells **15** specifically engages the orthosteric site of CB_2R prior to delivery of its cargo at the binding site periphery.

CONCLUSION

We reported herein novel synthetic access to a set of LDC probes incorporating *O*-NBD, *N*-sulfonyl pyridone (*N*-SP) and *N*-acyl-*N*-alkyl sulfonamide (NASA) electrophiles, which allowed covalent labeling of CB_2R *in vitro*, in HEK293 hCB_2R T-REx and AtT-20(SNAP-hCB2R) live cells. With the aid of computational docking and molecular dynamics simulations, nucleophilic lysine residues were identified, peripheral to CB_2R ligand binding site, suitable for affinity-driven covalent modification. The *in silico* inspired design of *O*-NBD probes **2a-e** yielded potent and selective CB_2R binders, as evaluated by a radioligand binding assay. Further profiling of **2a-e** by a fluorogenic TR-FRET assay allowed rapid confirmation of their potential to transfer NBD in a covalent fashion to a lysine residue of CB_2R. The *N*-SP and NASA electrophiles were incorporated into the probe design to enable delivery of fluorophores suitable for cellular experiments. New convergent synthetic strategies were developed and successfully implemented to achieve *N*-SP and NASA probes **11e** and **15** which bear a non-commercial CB_2R targeting ligand **1a** and a red-shifted fluorophore, DY-480XL. As judged by the *in vitro* TR-FRET assay, both probes achieve complete covalent labeling of CB_2R, with probe **15** demonstrating superior rate of covalent modification. The best performing probes of each electrophile class, **2b**, **11e**, **15**, were tested in live cells by

conventional and imaging flow cytometry experiments. DY-480XL functionalized probes **11e** and **15** demonstrated excellent specificity of binding to CB_2R as implied by comparison of CB_2R expressing HEK293 T-REx cells to wild-type cells across a range of concentrations. Imaging flow cytometry experiments with **11e** and **15** demonstrated clear visualization of plasma membrane bound CB_2R, which could be effectively blocked by pre-treatment with a CB_2R-selective competitive ligand SR-144,528. Furthermore, target specificity was corroborated by colocalization studies performed with **15** in AtT-20(SNAP-hCB_2R) cells. Finally, binding of **15** to the orthosteric site of CB_2R prior to cargo delivery at the receptor's periphery was validated in AtT-20(SNAP-hCB_2R) cells by pre-incubation with SR-144,528 and supported the ligand-driven nature of covalent labeling.

The NASA probe **15** demonstrated superior rate of labeling in comparison to its best performing *N*-SP counterpart **11e**. It is important to note that the choice of a suitable electrophile is guided by the target protein and availability of nucleophilic amino acid residues proximal to the binding site. The *N*-SP and NASA preference for tyrosine and lysine residues, respectively, makes the LDC platform a complementary toolbox to investigate a vast space of protein targets by covalent modifications. Consequently, the convergent synthetic blueprint effectively expands the possibilities of covalent modification with respect to both deliverable cargoes and proteome targetable with non-commercial ligands.

The need for reliable tools to study CB_2R is emphasized by the growing evidence of the receptor's crucial role in a plethora of neuroinflammatory diseases. For example, the lifetime, trafficking and recycling of CB_2R, which are poorly understood, may be studied and elucidated with LDC probes. We have reported the first probes to facilitate investigation of CB_2R by LDC chemistry using our agonist ligand **1a**.[35] The study of a cellular setting with minimal perturbation (no agonist induced receptor internalization) would demand an antagonist ligand. Unfortunately, to date no antagonist ligand with sufficient selectivity and specificity for CB_2R has been reported.[84] Once discovered, our novel synthetic platform promises to allow streamlined installation of a suitable CB_2R targeting antagonist ligand to **14**. The fluorescent probes, chemistry and analytical methods described herein will find valuable application both in the research of CB_2R and in the study of other protein targets by translation.

CONFLICT OF INTEREST

The authors declare the following competing financial interest: M.K., R.C.S., R.L.G., W.G., U.G. and E.M.C have filed a patent on CB_2R selective LDC probes.

CORRESPONDING AUTHORS

*E-mail: erickm.carreira@org.chem.ethz.ch

*E-mail: dmitry.veprintsev@nottingham.ac.uk

*E-mail: frankja@ohsu.edu

*E-mail: uwe.grether@roche.com

ACKNOWLEDGEMENTS

We are grateful to Björn Wagner for generating ASTA data and Isabelle Kaufmann for help with logistics. We thank René Arnold, Rainer Frankenstein and Stephan Burkhardt for their help with NMR measurements and the MoBiAS team for MS analysis. M.K. and R.C.S. gratefully acknowledge a fellowship by the Scholarship Fund of the Swiss Chemical Industry (SSCI). MD studies have been funded by project code PIR01_00011 "IBISCo", PON 2014-2020, for all three entities (INFN, UNINA and CNR). The ID7000C spectral cell analyzer was funded by the Biotechnology and Biological Sciences Research Council (BB/T017619/1). The ImageStreamX MKII imaging flow cytometer was funded by the Wellcome Trust (212908/Z/18/Z).

REFERENCES

1. Munro, S.; Thomas, K. L.; Abu-Shaar, M. Molecular characterization of a peripheral receptor for cannabinoids. *Nature* **1993**, *365* (*6441*), 61-65

2. Maccarrone, M. *New Tools to Interrogate Endocannabinoid Signalling: From Natural Compounds to Synthetic Drugs*; The Royal Society of Chemistry, 2021.

3. Galiegue, S.; Mary, S.; Marchand, J.; Dussossoy, D.; Carriere, D.; Carayon, P.; Bouaboula, M.; Shire, D.; Le Fur, G.; Casellas, P. Expression of central and peripheral cannabinoid receptors in human immune tissues and leukocyte subpopulations. *Eur. J. Biochem.* **1995**, *232* (*1*), 54-61

4. Svizenska, I.; Dubovy, P.; Sulcova, A. Cannabinoid receptors 1 and 2 (CB1 and CB2), their distribution, ligands and functional involvement in nervous system structures – a short review. *Pharmacol., Biochem. Behav.* **2008**, *90* (*4*), 501-511

5. Turcotte, C.; Blanchet, M. R.; Laviolette, M.; Flamand, N. The CB2 receptor and its role as a regulator of inflammation. *Cell. Mol. Life Sci.* **2016**, *73* (*23*), 4449-4470

6. Guindon, J.; Hohmann, A. G. Cannabinoid CB2 receptors: a therapeutic target for the treatment of inflammatory and neuropathic pain. *Br. J. Pharmacol.* **2008**, *153* (*2*), 319-334

7. Pacher, P.; Mechoulam, R. Is lipid signaling through cannabinoid 2 receptors part of a protective system? *Prog. Lipid Res.* **2011**, *50* (*2*), 193-211

8. Dhopeshwarkar, A.; Mackie, K. CB2 Cannabinoid receptors as a therapeutic target-what does the future hold? *Mol. Pharmacol.* **2014**, *86* (*4*), 430-437

9. Pacher, P.; Kunos, G. Modulating the endocannabinoid system in human health and disease--successes and failures. *FEBS J.* **2013**, *280* (*9*), 1918-1943

10. Schatz, A. R.; Lee, M.; Condie, R. B.; Pulaski, J. T.; Kaminski, N. E. Cannabinoid Receptors CB1 and CB2: a characterization of expression and adenylate cyclase modulation within the immune system. *Toxicol. Appl. Pharmacol.* **1997**, *142* (*2*), 278-287

11. Griffin, G.; Fernando, S. R.; Ross, R. A.; McKay, N. G.; Ashford, M. L.; Shire, D.; Huffman, J. W.; Yu, S.; Lainton, J. A.; Pertwee, R. G. Evidence for the presence of CB2-like cannabinoid receptors on peripheral nerve terminals. *Eur. J. Pharmacol.* **1997**, *339* (*1*), 53-61

12. Viscomi, M. T.; Oddi, S.; Latini, L.; Pasquariello, N.; Florenzano, F.; Bernardi, G.; Molinari, M.; Maccarrone, M. Selective CB2 receptor agonism protects central neurons from remote axotomy-induced apoptosis through the PI3K/Akt pathway. *J. Neurosci. Res.* **2009**, *29* (*14*), 4564-4570

13. Stempel, A. V.; Stumpf, A.; Zhang, H. Y.; Ozdogan, T.; Pannasch, U.; Theis, A. K.; Otte, D. M.; Wojtalla, A.; Racz, I.; Ponomarenko, A.; Xi, Z. X.; Zimmer, A.; Schmitz, D. Cannabinoid Type 2 Receptors Mediate a Cell Type-Specific Plasticity in the Hippocampus. *Neuron* **2016**, *90* (*4*), 795-809

14. Li, Y.; Kim, J. Neuronal expression of CB2 cannabinoid receptor mRNAs in the mouse hippocampus. *Neuroscience* **2015**, *311*, 253-267

15. Lanciego, J. L.; Barroso-Chinea, P.; Rico, A. J.; Conte-Perales, L.; Callen, L.; Roda, E.; Gomez-Bautista, V.; Lopez, I. P.; Lluis, C.; Labandeira-Garcia, J. L.; Franco, R. Expression of the

mRNA coding the cannabinoid receptor 2 in the pallidal complex of Macaca fascicularis. *J. Psychopharmacol.* **2011**, *25* (*1*), 97-104

16. Garcia-Gutierrez, M. S.; Garcia-Bueno, B.; Zoppi, S.; Leza, J. C.; Manzanares, J. Chronic blockade of cannabinoid CB2 receptors induces anxiolytic-like actions associated with alterations in GABA(A) receptors. *Br. J. Pharmacol.* **2012**, *165* (*4*), 951-964

17. Cabral, G. A.; Raborn, E. S.; Griffin, L.; Dennis, J.; Marciano-Cabral, F. CB2 receptors in the brain: role in central immune function. *Br. J. Pharmacol.* **2008**, *153* (*2*), 240-251

18. Stella, N. Cannabinoid and cannabinoid-like receptors in microglia, astrocytes, and astrocytomas. *Glia* **2010**, *58* (*9*), 1017-1030

19. Cabral, G. A.; Marciano-Cabral, F. Cannabinoid receptors in microglia of the central nervous system: immune functional relevance. *J. Leukocyte Biol.* **2005**, *78* (*6*), 1192-1197

20. Rivers, J. R.; Ashton, J. C. The development of cannabinoid CBII receptor agonists for the treatment of central neuropathies. *Cent. Nerv. Syst. Agents Med. Chem.* **2010**, *10* (*1*), 47-64

21. Little, J. P.; Villanueva, E. B.; Klegeris, A. Therapeutic potential of cannabinoids in the treatment of neuroinflammation associated with Parkinson's disease. *Mini-Rev. Med. Chem.* **2011**, *11* (*7*), 582-590

22. *c.w.Biorender*.

23. Concannon, R. M.; Okine, B. N.; Finn, D. P.; Dowd, E. Upregulation of the cannabinoid CB2 receptor in environmental and viral inflammation-driven rat models of Parkinson's disease. *Exp. Neurol.* **2016**, *283* (*Pt A*), 204-212

24. Aso, E.; Ferrer, I. CB2 Cannabinoid Receptor As Potential Target against Alzheimer's Disease. *Front Neurosci* **2016**, *10*, 243

25. Cecyre, B.; Thomas, S.; Ptito, M.; Casanova, C.; Bouchard, J. F. Evaluation of the specificity of antibodies raised against cannabinoid receptor type 2 in the mouse retina. *Naunyn Schmiedebergs Arch Pharmacol* **2014**, *387* (*2*), 175-84

26. Marchalant, Y.; Brownjohn, P. W.; Bonnet, A.; Kleffmann, T.; Ashton, J. C. Validating Antibodies to the Cannabinoid CB2 Receptor: Antibody Sensitivity Is Not Evidence of Antibody Specificity. *J. Histochem. Cytochem.* **2014**, *62* (*6*), 395-404

27. Zhang, H. Y.; Shen, H.; Jordan, C. J.; Liu, Q. R.; Gardner, E. L.; Bonci, A.; Xi, Z. X. CB2 receptor antibody signal specificity: correlations with the use of partial CB2-knockout mice and anti-rat CB2 receptor antibodies. *Acta Pharmacol. Sin.* **2019**, *40* (*3*), 398-409

28. Brownjohn, P. W.; Ashton, J. C. Spinal cannabinoid CB2 receptors as a target for neuropathic pain: an investigation using chronic constriction injury. *Neuroscience* **2012**, *203*, 180-193

29. Gazzi, T.; Brennecke, B.; Atz, K.; Korn, C.; Sykes, D.; Forn-Cuni, G.; Pfaff, P.; Sarott, R. C.; Westphal, M. V.; Mostinski, Y.; Mach, L.; Wasinska-Kalwa, M.; Weise, M.; Hoare, B. L.; Miljuš, T.; Mexi, M.; Roth, N.; Koers, E. J.; Guba, W.; Alker, A.; Rufer, A. C.; Kusznir, E. A.; Huber, S.; Raposo, C.; Zirwes, E. A.; Osterwald, A.; Pavlovic, A.; Moes, S.; Beck, J.; Nettekoven, M.; Benito-Cuesta, I.; Grande, T.; Drawnel, F.; Widmer, G.; Holzer, D.; van der Wel, T.; Mandhair, H.; Honer, M.; Fingerle, J.; Scheffel, J.; Broichhagen, J.; Gawrisch, K.; Romero, J.; Hillard, C. J.; Varga, Z. V.; van der Stelt, M.; Pacher, P.; Gertsch, J.; Ullmer, C.; McCormick, P. J.; Oddi, S.; Spaink, H. P.; Maccarrone, M.; Veprintsev, D. B.; Carreira, E. M.; Grether, U.; Nazaré, M. Detection of cannabinoid receptor type 2 in native cells and zebrafish with a highly potent, cell-permeable fluorescent probe. *Chem. Sci.* **2022**, *13* (*19*), 5539-5545

30. Sarott, R. C.; Westphal, M. V.; Pfaff, P.; Korn, C.; Sykes, D. A.; Gazzi, T.; Brennecke, B.; Atz, K.; Weise, M.; Mostinski, Y.; Hompluem, P.; Koers, E.; Miljus, T.; Roth, N. J.; Asmelash, H.; Vong, M. C.; Piovesan, J.; Guba, W.; Rufer, A. C.; Kusznir, E. A.; Huber, S.; Raposo, C.; Zirwes, E. A.; Osterwald, A.; Pavlovic, A.; Moes, S.; Beck, J.; Benito-Cuesta, I.; Grande, T.; Ruiz de Marti, N. E. S.; Yeliseev, A.; Drawnel, F.; Widmer, G.; Holzer, D.; van der Wel, T.; Mandhair, H.; Yuan, C. Y.; Drobyski, W. R.; Saroz, Y.; Grimsey, N.; Honer, M.; Fingerle, J.; Gawrisch, K.; Romero, J.; Hillard, C. J.; Varga, Z. V.; van der Stelt, M.; Pacher, P.; Gertsch, J.; McCormick, P. J.; Ullmer, C.; Oddi, S.; Maccarrone, M.; Veprintsev, D. B.; Nazare, M.; Grether, U.; Carreira, E. M. Development of High-Specificity Fluorescent Probes to Enable Cannabinoid Type 2 Receptor Studies in Living Cells. *J. Am. Chem. Soc.* **2020**, *142* (*40*), 16953-16964

31. Cooper, A.; Singh, S.; Hook, S.; Tyndall, J. D. A.; Vernall, A. J. Chemical Tools for Studying Lipid-Binding Class A G Protein-Coupled Receptors. *Pharmacol. Rev.* **2017**, *69* (*3*), 316-353

32. Chen, D. J.; Gao, M.; Gao, F. F.; Su, Q. X.; Wu, J. Brain cannabinoid receptor 2: expression, function and modulation. *Acta Pharmacol. Sin.* **2017**, *38* (*3*), 312-316

33. Grimsey, N. L.; Goodfellow, C. E.; Dragunow, M.; Glass, M. Cannabinoid receptor 2 undergoes Rab5-mediated internalization and recycles via a Rab11-dependent pathway. *Biochim. Biophys. Acta* **2011**, *1813* (*8*), 1554-1560

34. Wang, L.; Frei, M. S.; Salim, A.; Johnsson, K. Small-Molecule Fluorescent Probes for Live-Cell Super-Resolution Microscopy. *J. Am. Chem. Soc.* **2019**, *141* (*7*), 2770-2781

35. Westphal, M. V.; Sarott, R. C.; Zirwes, E. A.; Osterwald, A.; Guba, W.; Ullmer, C.; Grether, U.; Carreira, E. M. Highly Selective, Amine-Derived Cannabinoid Receptor 2 Probes. *Chem. Eur. J.* **2020**, *26* (*6*), 1380-1387

36. Hayashi, T.; Hamachi, I. Traceless affinity labeling of endogenous proteins for functional analysis in living cells. *Acc. Chem. Res.* **2012**, *45* (*9*), 1460-1469

37. Tamura, T.; Hamachi, I. Chemistry for Covalent Modification of Endogenous/Native Proteins: From Test Tubes to Complex Biological Systems. *J. Am. Chem. Soc.* **2019**, *141* (*7*), 2782-2799

38. Wold, F. Affinity labeling--an overview. *Methods Enzymol.* **1977**, *46*, 3-14

39. Fujishima, S. H.; Yasui, R.; Miki, T.; Ojida, A.; Hamachi, I. Ligand-directed acyl imidazole chemistry for labeling of membrane-bound proteins on live cells. *J. Am. Chem. Soc.* **2012**, *134* (*9*), 3961-3964

40. Hughes, C. C.; Yang, Y. L.; Liu, W. T.; Dorrestein, P. C.; La Clair, J. J.; Fenical, W. Marinopyrrole A target elucidation by acyl dye transfer. *J. Am. Chem. Soc.* **2009**, *131* (*34*), 12094-12096

41. Jing, C.; Cornish, V. W. A fluorogenic TMP-tag for high signal-to-background intracellular live cell imaging. *ACS Chem. Biol.* **2013**, *8* (*8*), 1704-1712

42. Kojima, H.; Fujita, Y.; Takeuchi, R.; Ikebe, Y.; Ohashi, N.; Yamamoto, K.; Itoh, T. Cyclization Reaction-Based Turn-on Probe for Covalent Labeling of Target Proteins. *Cell Chem. Biol.* **2020**, *27* (*3*), 334-349

43. Masuya, T.; Murai, M.; Ifuku, K.; Morisaka, H.; Miyoshi, H. Site-specific chemical labeling of mitochondrial respiratory complex I through ligand-directed tosylate chemistry. *Biochemistry* **2014**, *53* (*14*), 2307-2317

44. Takaoka, Y.; Nishikawa, Y.; Hashimoto, Y.; Sasaki, K.; Hamachi, I. Ligand-directed dibromophenyl benzoate chemistry for rapid and selective acylation of intracellular natural proteins. *Chem. Sci.* **2015**, *6* (*5*), 3217-3224

45. Tamura, T.; Tsukiji, S.; Hamachi, I. Native FKBP12 engineering by ligand-directed tosyl chemistry: labeling properties and application to photo-cross-linking of protein complexes in vitro and in living cells. *J. Am. Chem. Soc.* **2012**, *134* (*4*), 2216-2226

46. Yamaura, K.; Kiyonaka, S.; Numata, T.; Inoue, R.; Hamachi, I. Discovery of allosteric modulators for GABAA receptors by ligand-directed chemistry. *Nat. Chem. Biol.* **2016**, *12* (*10*), 822-830

47. Zhang, X.; Jiang, L.; Huang, K.; Fang, C.; Li, J.; Yang, J.; Li, H.; Ruan, X.; Wang, P.; Mo, M.; Wu, P.; Xu, Y.; Peng, C.; Uesugi, M.; Ye, D.; Yu, F. X.; Zhou, L. Site-Selective Phosphoglycerate Mutase 1 Acetylation by a Small Molecule. *ACS Chem. Biol.* **2020**, *15* (*3*), 632-639

48. Arttamangkul, S.; Plazek, A.; Platt, E. J.; Jin, H.; Murray, T. F.; Birdsong, W. T.; Rice, K. C.; Farrens, D. L.; Williams, J. T. Visualizing endogenous opioid receptors in living neurons using ligand-directed chemistry. *eLife* **2019**, *8*,

49. Tamura, T.; Song, Z.; Amaike, K.; Lee, S.; Yin, S.; Kiyonaka, S.; Hamachi, I. Affinity-Guided Oxime Chemistry for Selective Protein Acylation in Live Tissue Systems. *J. Am. Chem. Soc.* **2017**, *139* (*40*), 14181-14191

50. Wakayama, S.; Kiyonaka, S.; Arai, I.; Kakegawa, W.; Matsuda, S.; Ibata, K.; Nemoto, Y. L.; Kusumi, A.; Yuzaki, M.; Hamachi, I. Chemical labelling for visualizing native AMPA receptors in live neurons. *Nat. Commun.* **2017**, *8*, 14850-14864

51. Tsukiji, S.; Miyagawa, M.; Takaoka, Y.; Tamura, T.; Hamachi, I. Ligand-directed tosyl chemistry for protein labeling in vivo. *Nat. Chem. Biol.* **2009**, *5* (*5*), 341-343

52. Matsuo, K.; Nishikawa, Y.; Masuda, M.; Hamachi, I. Live-Cell Protein Sulfonylation Based on Proximity-driven N-Sulfonyl Pyridone Chemistry. *Angew. Chem., Int. Ed.* **2018**, *57* (*3*), 659-662

53. Tamura, T.; Ueda, T.; Goto, T.; Tsukidate, T.; Shapira, Y.; Nishikawa, Y.; Fujisawa, A.; Hamachi, I. Rapid labelling and covalent inhibition of intracellular native proteins using ligand-directed *N*-acyl-*N*-alkyl sulfonamide. *Nat. Commun.* **2018**, *9* (*1*), 1870-1882

54. Ireland, R. E. *Organic Synthesis*; Prentice-Hall, 1969.

55. Crispino, G. A.; Ho, P. T.; Sharpless, K. B. Selective perhydroxylation of squalene: taming the arithmetic demon. *Science* **1993**, *259* (*5091*), 64-66

56. Mortensen, M. R.; Skovsgaard, M. B.; Gothelf, K. V. Considerations on Probe Design for Affinity-Guided Protein Conjugation. *ChemBioChem* **2019**, *20* (*21*), 2711-2728

57. Shiraiwa, K.; Cheng, R.; Nonaka, H.; Tamura, T.; Hamachi, I. Chemical Tools for Endogenous Protein Labeling and Profiling. *Cell Chem. Biol.* **2020**, *27* (*8*), 970-985

58. Vernall, A. J.; Stoddart, L. A.; Briddon, S. J.; Ng, H. W.; Laughton, C. A.; Doughty, S. W.; Hill, S. J.; Kellam, B. Conversion of a non-selective adenosine receptor antagonist into A3-selective high affinity fluorescent probes using peptide-based linkers. *Org. Biomol. Chem.* **2013**, *11* (*34*), 5673-5682

59. Sexton, M.; Woodruff, G.; Horne, E. A.; Lin, Y. H.; Muccioli, G. G.; Bai, M.; Stern, E.; Bornhop, D. J.; Stella, N. NIR-mbc94, a fluorescent ligand that binds to endogenous CB(2) receptors and is amenable to high-throughput screening. *Chem. Biol.* **2011**, *18* (*5*), 563-568

60. Cooper, A. G.; MacDonald, C.; Glass, M.; Hook, S.; Tyndall, J. D. A.; Vernall, A. J. Alkyl indole-based cannabinoid type 2 receptor tools: Exploration of linker and fluorophore attachment. *Eur. J. Med. Chem.* **2018**, *145*, 770-789

61. Baker, J. G.; Middleton, R.; Adams, L.; May, L. T.; Briddon, S. J.; Kellam, B.; Hill, S. J. Influence of fluorophore and linker composition on the pharmacology of fluorescent adenosine A1 receptor ligands. *Br. J. Pharmacol.* **2010**, *159* (*4*), 772-786

62. Pettinger, J.; Jones, K.; Cheeseman, M. D. Lysine-Targeting Covalent Inhibitors. *Angew. Chem. Int. Ed.* **2017**, *56* (*48*), 15200-15209

63. Yamaguchi, T.; Asanuma, M.; Nakanishi, S.; Saito, Y.; Okazaki, M.; Dodo, K.; Sodeoka, M. Turn-ON fluorescent affinity labeling using a small bifunctional O-nitrobenzoxadiazole unit. *Chem. Sci.* **2014**, *5* (*3*), 1021-1029

64. Uchiyama, S.; Takehira, K.; Kohtani, S.; Imai, K.; Nakagaki, R.; S., T.; T., S. Fluorescence on–off switching mechanism of benzofurazans. *Org. Biomol. Chem.* **2003**, *1* (*6*), 1067-1072

65. Uchiyama, S.; Santa, T.; Fukushima, T.; Homma, H.; Imai, K. Effects of the substituent groups at the 4- and 7-positions on the fluorescence characteristics of benzofurazan compounds. *J. Chem. Soc., Perkin Trans. 2* **1998**, (*10*), 2165-2174

66. Xing, C.; Zhuang, Y.; Xu, T. H.; Feng, Z.; Zhou, X. E.; Chen, M.; Wang, L.; Meng, X.; Xue, Y.; Wang, J.; Liu, H.; McGuire, T. F.; Zhao, G.; Melcher, K.; Zhang, C.; Xu, H. E.; Xie, X. Q. Cryo-EM Structure of the Human Cannabinoid Receptor CB2-Gi Signaling Complex. *Cell* **2020**, *180* (*4*), 645-654

67. Xue, D.; Ye, L.; Zheng, J.; Wu, Y.; Zhang, X.; Xu, Y.; Li, T.; Stevens, R. C.; Xu, F.; Zhuang, M.; Zhao, S.; Zhao, F.; Tao, H. The structure-based traceless specific fluorescence labeling of the smoothened receptor. *Org. Biomol. Chem.* **2019**, *17* (*25*), 6136-6142

68. Li, X.; Hua, T.; Vemuri, K.; Ho, J. H.; Wu, Y.; Wu, L.; Popov, P.; Benchama, O.; Zvonok, N.; Locke, K.; Qu, L.; Han, G. W.; Iyer, M. R.; Cinar, R.; Coffey, N. J.; Wang, J.; Wu, M.; Katritch, V.; Zhao, S.; Kunos, G.; Bohn, L. M.; Makriyannis, A.; Stevens, R. C.; Liu, Z. J. Crystal Structure of the Human Cannabinoid Receptor CB2. *Cell* **2019**, *176* (*3*), 459-467

69. Jo, S.; Kim, T.; Iyer, V. G.; Im, W. CHARMM-GUI: a web-based graphical user interface for CHARMM. *J. Comput. Chem.* **2008**, *29* (*11*), 1859-1865

70. Wu, E. L.; Cheng, X.; Jo, S.; Rui, H.; Song, K. C.; Davila-Contreras, E. M.; Qi, Y.; Lee, J.; Monje-Galvan, V.; Venable, R. M.; Klauda, J. B.; Im, W. CHARMM-GUI Membrane Builder toward realistic biological membrane simulations. *J. Comput. Chem.* **2014**, *35* (*27*), 1997-2004

71. Case, D. A.; Aktulga, H. M.; Belfon, K.; Ben-Shalom, I. Y.; Berryman, J. T.; Brozell, S. R.; Cerutti, D. S.; Cheatham, I., T.E.; Cisneros, G. A.; Cruzeiro, V. W. D.; Darden, T. A.; Duke, R. E.; Giambasu, G.; Gilson, M. K.; Gohlke, H.; Goetz, A. W.; Harris, R.; Izadi, S.; Izmailov, S. A.; Kasavajhala, K.; Kaymak, M. C.; King, E.; Kovalenko, A.; Kurtzman, T.; Lee, T. S.; LeGrand, S.; Li, P.; Lin, C.; Liu, J.; Luchko, T.; Luo, R.; Machado, M.; Man, V.; Manathunga, M.; Merz, K. M.; Miao, Y.; Mikhailovskii, O.; Monard, G.; Nguyen, H.; O'Hearn, K. A.; Onufriev, A.; Pan, F.; Pantano, S.; Qi, R.; Rahnamoun, A.; Roe, D. R.; Roitberg, A.; Sagui, C.; Schott-Verdugo, S.; Shajan, A.; Shen, J.; Simmerling, C. L.; Skrynnikov, N. R.; Smith, J.; Swails, J.; Walker, R. C.; Wang, J.; Wang, J.; Wei, H.; Wolf, R. M.; Wu, X.; Xiong, Y.; Xue, Y.; York, D. M.; Zhao, S.; Kollman, P. A. *Amber* **2022**, *University of California, San Francisco*,

72. Hua, T.; Li, X.; Wu, L.; Iliopoulos-Tsoutsouvas, C.; Wang, Y.; Wu, M.; Shen, L.; Brust, C. A.; Nikas, S. P.; Song, F.; Song, X.; Yuan, S.; Sun, Q.; Wu, Y.; Jiang, S.; Grim, T. W.; Benchama, O.; Stahl, E. L.; Zvonok, N.; Zhao, S.; Bohn, L. M.; Makriyannis, A.; Liu, Z. J. Activation and Signaling Mechanism Revealed by Cannabinoid Receptor-Gi Complex Structures. *Cell* **2020**, *180* (*4*), 655-665

73. Reddi, R. N.; Rogel, A.; Resnick, E.; Gabizon, R.; Prasad, P. K.; Gurwicz, N.; Barr, H.; Shulman, Z.; London, N. Site-Specific Labeling of Endogenous Proteins Using CoLDR Chemistry. *J. Am. Chem. Soc.* **2021**, *143* (*48*), 20095-20108

74. Tamura, T.; Kioi, Y.; Miki, T.; Tsukiji, S.; Hamachi, I. Fluorophore labeling of native FKBP12 by ligand-directed tosyl chemistry allows detection of its molecular interactions *in vitro* and in living cells. *J. Am. Chem. Soc.* **2013**, *135* (*18*), 6782-6785

75. Stoddart, L. A.; Kindon, N. D.; Otun, O.; Harwood, C. R.; Patera, F.; Veprintsev, D. B.; Woolard, J.; Briddon, S. J.; Franks, H. A.; Hill, S. J.; Kellam, B. Ligand-directed covalent labelling of a GPCR with a fluorescent tag in live cells. *Commun. Biol.* **2020**, *3* (*1*), 722-731

76. Soethoudt, M.; Grether, U.; Fingerle, J.; Grim, T. W.; Fezza, F.; de Petrocellis, L.; Ullmer, C.; Rothenhausler, B.; Perret, C.; van Gils, N.; Finlay, D.; MacDonald, C.; Chicca, A.; Gens, M. D.; Stuart, J.; de Vries, H.; Mastrangelo, N.; Xia, L.; Alachouzos, G.; Baggelaar, M. P.; Martella, A.; Mock, E. D.; Deng, H.; Heitman, L. H.; Connor, M.; Di Marzo, V.; Gertsch, J.; Lichtman, A. H.; Maccarrone, M.; Pacher, P.; Glass, M.; van der Stelt, M. Cannabinoid CB2 receptor ligand profiling reveals biased signalling and off-target activity. *Nat. Commun.* **2017**, *8*, 13958-13972

77. Benson, D. M.; Bryan, J.; Plant, A. L.; Gotto, A. M., Jr.; Smith, L. C. Digital imaging fluorescence microscopy: spatial heterogeneity of photobleaching rate constants in individual cells. *J. Cell Biol.* **1985**, *100* (*4*), 1309-1323

78. Thimaradka, V.; Hoon Oh, J.; Heroven, C.; Radu Aricescu, A.; Yuzaki, M.; Tamura, T.; Hamachi, I. Site-specific covalent labeling of His-tag fused proteins with N-acyl-N-alkyl sulfonamide reagent. *Bioorg. Med. Chem.* **2021**, *30*, 115947-115953

79. Tivon, Y.; Falcone, G.; Deiters, A. Protein Labeling and Crosslinking by Covalent Aptamers. *Angew. Chem. Int. Ed.* **2021**, *60* (*29*), 15899-15904

80. Ueda, T.; Tamura, T.; Hamachi, I. Development of a Cell-Based Ligand-Screening System for Identifying Hsp90 Inhibitors. *Biochemistry* **2020**, *59* (*2*), 179-182

81. Ueda, T.; Tamura, T.; Kawano, M.; Shiono, K.; Hobor, F.; Wilson, A. J.; Hamachi, I. Enhanced Suppression of a Protein-Protein Interaction in Cells Using Small-Molecule Covalent Inhibitors Based on an N-Acyl-N-alkyl Sulfonamide Warhead. *J. Am. Chem. Soc.* **2021**, *143* (*12*), 4766-4774

82. Teng, M.; Jiang, J.; Ficarro, S. B.; Seo, H. S.; Bae, J. H.; Donovan, K. A.; Fischer, E. S.; Zhang, T.; Dhe-Paganon, S.; Marto, J. A.; Gray, N. S. Exploring Ligand-Directed N-Acyl-N-alkylsulfonamide-Based Acylation Chemistry for Potential Targeted Degrader Development. *ACS Med. Chem. Lett.* **2021**, *12* (*8*), 1302-1307

83. Natasha S. Barteneva, I. A. V. *Imaging Flow Cytometry*; Humana New York, 2016.

84. Singh, S.; Oyagawa, C. R. M.; Macdonald, C.; Grimsey, N. L.; Glass, M.; Vernall, A. J. Chromenopyrazole-based High Affinity, Selective Fluorescent Ligands for Cannabinoid Type 2 Receptor. *ACS Med. Chem. Lett.* **2019**, *10* (*2*), 209-214. The single inverse agonist probe, in a

series of agonist probes with the same ligand, owes its functional profile to a specific linker length and fluorophore.